THE DETECTOR SIGNAL PROCESSING CHAIN OF THE ISO LONG WAVELENGTH SPECTROMETER

C. DELETTREZ [1,3], M. J. GRIFFIN [2], C. LE NAOUR [1,4], S. CHURCH [2], J-P. CHABAUD [1]

[1] *Centre d'Etude Spatiale des Rayonnements (CNRS - UPS)*
9, Avenue du Colonel Roche, B.P. 4346, 31029 - Toulouse Cédex, France.

[2] *Queen Mary and Westfield College*
Mile End Road, London, E1 4NS, England.

[3] *presently at MATRA MARCONI SPACE FRANCE (M.M.S. - F)*
31, rue des Cosmonautes, ZI du Palays, 31077 - Toulouse Cédex, France

[4] *presently at Centre National d'Etudes Spatiales (CNES)*
18, Avenue Edouard Belin, 31055 - Toulouse Cédex, France

(Received 1 April 1993; accepted 21 Decmber 1993)

Abstract. This paper describes the analogue signal processing chain for the detectors in the Long Wavelength Spectrometer (LWS) to be flown on board the Infrared Space Observatory (ISO) satellite. The satellite, its mission, and the on-board experiments are briefly reviewed, and the configuration of the LWS Detector Subsystem is described. Two possible signal readout and amplification schemes, based on the Transimpedance Amplifier (TIA) and the Integrating Amplifier (IA) are discussed. The reasons for the choice of the IA for the LWS are outlined. The design of the complete LWS detector signal chain is presented.

1. Introduction

The Earth's atmosphere is opaque over most of the far infrared (FIR) region. Ground-based observations are impossible, except in a few low-transparency window regions, in which sensitivity is limited by the thermal emission of the atmosphere and the warm telescope. Previous space missions such as the Infrared Astronomy Satellite (IRAS) in 1983 (Langford et al., 1983) and the Spacelab 2 Infrared Telescope in 1985 (Young et al., 1981) have proved the value of astronomical observations in the FIR.

Experimental Astronomy 4: 213–235, 1994.

The next major satellite-borne FIR mission will be the ESA Infrared Space Observatory - ISO (Emery et al., 1987; Eggel et al., 1990). Due to be launched in April 1995, this satellite will carry a 60-cm telescope and four focal plane instruments. They will be cooled by a toroidal tank of about 2000 litres of superfluid helium. The mission lifetime will be 18 months or more. The observatory will provide the international astronomical community with a complementary set of instruments for imaging (ISOCAM), photometry (ISOPHOT) and spectroscopy. The two on-board spectrometers, the SWS (Short Wavelength Spectrometer) and the LWS (Long Wavelength Spectrometer) jointly cover the range from 3 to 180 μm. The LWS experiment operates in the upper wavelengths, from 45 to 180 μm. This experiment is built by an international consortium of research laboratories, led by Prof. P.E. Clegg, Principal Investigator. The QMW laboratory has the responsibility for the LWS detector subsystem, while CESR is in charge of the design, manufacture and qualification of the warm analogue electronics (APU).

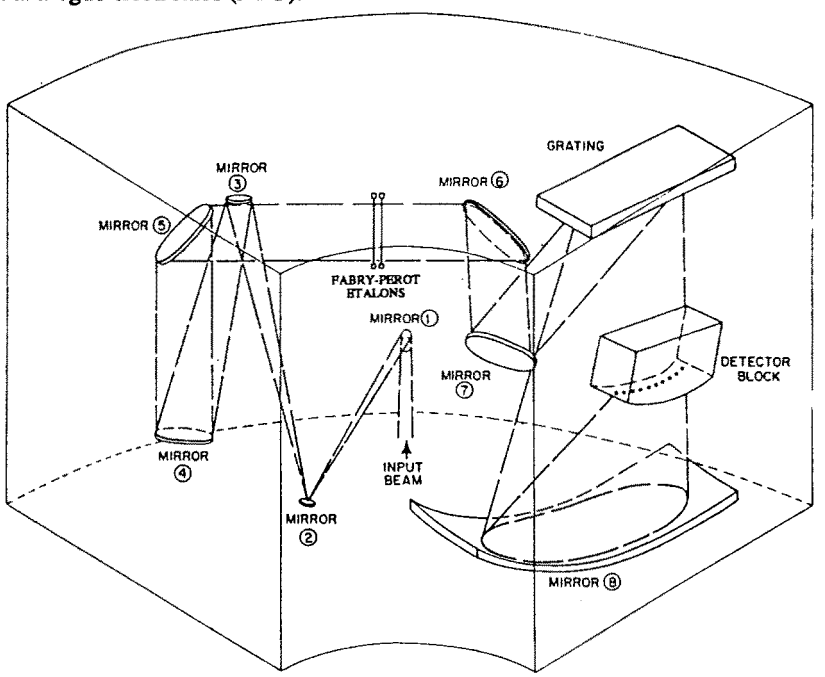

Figure 1

Schematic diagram of the LWS.

Figure 1 is a schematic diagram of the LWS. A reflection grating is used to provide medium-resolution ($\lambda/\Delta\lambda \approx 200$) spectrometry. To operate the instrument in high-resolution mode ($\lambda/\Delta\lambda \approx 10000$), one of two selectable Fabry-Perot interferometers is placed in the beam, the grating then being used to order-sort the Fabry-Perot. One F-P is optimised for the 45 to 90 μm region, and the other for 90 to 180 μm.

The LWS has a linear array of ten gallium-doped germanium photoconductive detectors. Each detector has the same 100" diameter field of view on the sky, but is sensitive in a different wavelength interval. Bandpass filters are used to define precisely the passband of each detector, and to order-sort the grating. In low-resolution mode, a spectrum is measured by scanning the grating over a few degrees, with all ten detectors operating simultaneously. For high-resolution observations, the Fabry-Perot and the grating are used together, and in that mode one detector is used at any one time.

The LWS instrument will operate at the ISO focal plane temperature of approximately 3 K, maintained by vapour-cooling from the helium boil-off. The LWS detectors are 1-mm^3 doped germanium photoconductors. For the shortest wavelength channel (45-50 μm), a Ge:Be detector is used. Five Ge:Ga detectors are used for 50-100 μm, and four stressed Ge:Ga detectors cover the 110-200 μm range. Two separate detector temperature stages are provided. The Ge:Be and unstressed Ge:Ga detectors operate at 3 K and the stressed detectors at 1.85 K. The stressed detector bar is connected directly by a copper strap to the superfluid helium tank, maintaining it at a fixed temperature. The unstressed detector bar has weak thermal links to the cold strap (1.85 K) and the instrument wall (3.5 K). Its temperature is maintained at 3 K by the on-board computer, with a stability of 5 mK.

The LWS instrument, the detector subsystem, and the characteristics and performances of the detectors, are described in detail by Griffin et al. (1990), Emery et al. (1992) and Church et al. (1992), and will not be repeated here.

The design of the detector readout, preamplification and signal processing chain is crucial to achieve the best possible overall sensitivity. The most important requirement is that the detector signals be regularly read out and digitised by the signal chain electronics without adding significantly to the total noise. This should be determined either by the detectors themselves or by photon noise from the incident FIR radiation. In addition, to minimise microphonic effects and electromagnetic interference (both of which can be severe with sensitive high-impedance detectors), the first stage of the amplification chain needs to be physically very close to the detector, and therefore must be capable of operating at cryogenic temperatures.

In Section 2, the design of the LWS Detector Subsystem is described. Sections 3 contains an account of the Transimpedance (TIA) amplifier originally adopted for the LWS. The Integrating Amplifier (IA) configuration and the reasons for its use in the final LWS design are discussed in Section 4. The complete LWS detector analogue signal conditioning chain is described in Section 5. Some test results on the LWS Flight Model are presented in Section 6.

2. The LWS Detector Subsystem

The Detector Subsystem (Griffin et al., 1990) is illustrated in Figure 2. The ten detectors are in a curved linear array along the focal line of the final spherical condensing mirror. Each detector is connected to a dual JFET integrating amplifier (IA), located just behind it on the subsystem block.

The IA output is fed to the LWS warm Analogue Processing Unit (APU) through a 5-m length stainless steel cryo-harness. Five infrared illuminators are attached to the instrument sidewall, and will be used to provide repeatable calibration signals for the detectors. This facility will be used to monitor and calibrate out any changes in overall system responsivity arising from ionising radiation effects on the detectors (on timescales of an orbit or less), or from ageing of components in the signal chain electronics (e.g., resulting in a slow change of the detector bias voltages over the lifetime of the mission).

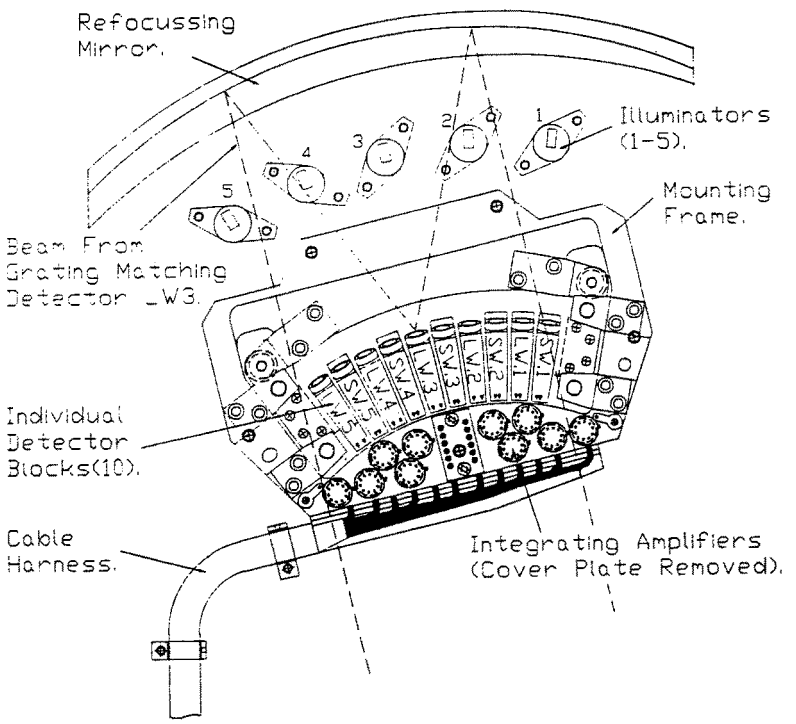

Figure 2

LWS Detector Subsystem (Front View)

A stressed detector mount is illustrated in Figure 3 (the unstressed mount is similar, but does not have the stressing screw). A light concentrator in front of the detector cavity allows each detector to view the grating with the required field of view. The spectral filter and detector aperture are located at the front of the block.

The LWS detectors are similar to those used in the IRAS 60 and 100 μm channels. But, because of the high spectral resolution of the LWS, the photon background on the detectors will be order of magnitude lower. Therefore, although the detectors themselves are similar, the operating conditions are very different. When the LWS detectors are operating in Fabry-Perot mode, the detector photocurrent can be comparable to, or smaller than, the detector dark current.

Ideally, the total noise should be dominated by statistical fluctuations in the detector dark current, and a form of signal readout with a read noise less than this limit is required.

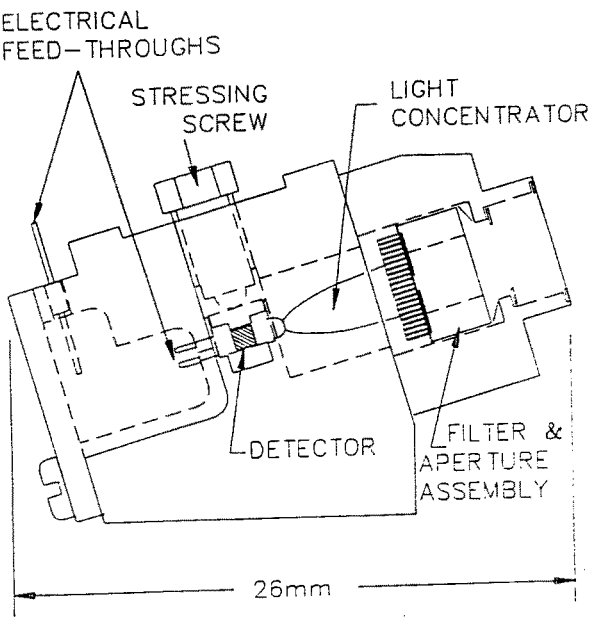

Figure 3

Stressed detector mount.

3. The Transimpedance Amplifier (TIA)

The first amplifier design considered for the LWS was the Transimpedance Amplifier (TIA). It has already been successfully used for many balloon-, aircraft-, and satellite-borne FIR instruments (e.g., Luinge et al., 1980), the most important being the IRAS mission (Langford et al., 1983). In the first instance, the TIA was adopted as the preamplifier design for the LWS.

One of the most important parameters of the TIA design is the configuration of the first stage FET(s). The most stable and reliable one uses a matched pair of FETs as the input stage. This provides minimum sensitivity to drifts in the characteristics of the FETs and to possible EM interference along the cryo-harness. Such a scheme was used for the IRAS satellite (Langford et al., 1983), and proved extremely successful.

IRAS used a dual JFET pair (Low, 1981) manufactured by Infrared Laboratories, based on the J-230 silicon JFET. This is a well known component with good characteristics. The reliability, stability and radiation hardness of the JFET-based TIA have been amply demonstrated by the IRAS mission. Its only disadvantage for cryogenic TIA operation is that the silicon JFETs do not conduct at temperatures below about 30 K. The JFET pair therefore needs to be thermally isolated from the focal plane, and heated internally to the optimum operating temperature of about 60 K. Other component technologies (MOS-FETs and GaAs-FETs) are available that allow operation at helium temperature, thereby simplifying the mechanical and thermal design and reducing the total power dissipation. In addition to being sensitive to damage by electrostatic discharge, MOSFETs exhibit DC instabilities at temperatures below 20 K, probably due to freezing out of carriers. They present also excessively high voltage noise (Low 1981; Young, 1983).

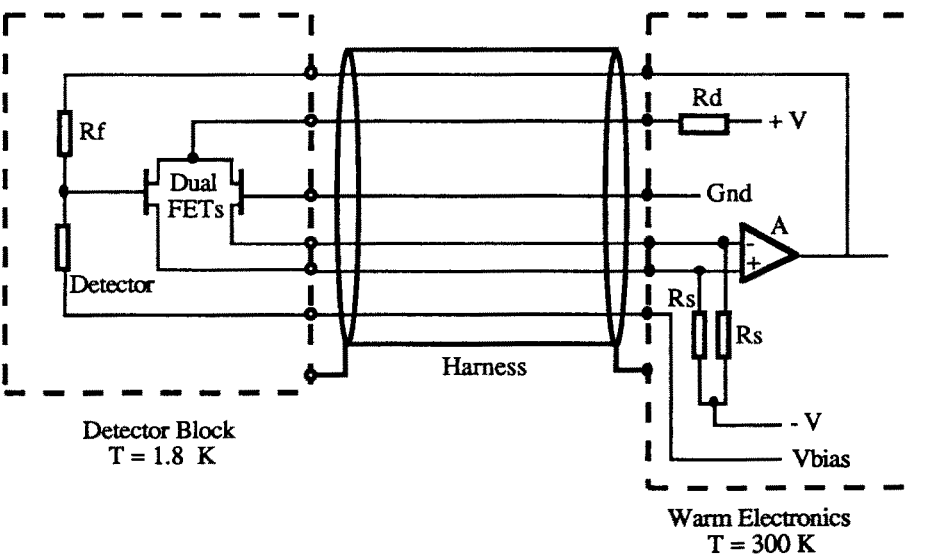

Figure 4

Dual GaAs-FETs TIA.

Overall View.

GaAs-FETs also can be operated at helium temperature with power dissipation less than 30 μW. They exhibit a higher degree of 1/f noise than JFETs. But, provided that the GaAs-FET noise is less than that of the feedback resistor, this will not limit the sensitivity in the TIA circuit. A suitable low noise GaAs-FET for helium temperature operation is the Plessey P35-1101. For the LWS TIA test programme, a specially made dual version was provided by Plessey, with well matched FETs mounted on a single substrate.

Figure 4 shows the LWS TIA circuit. It is almost identical to the IRAS circuit described by Langford et al. (1983), except for the use of GaAs-FETs. The nominal components values were as follows:

V	$\approx \pm 15$ V	
V_{Bias}	= 50 - 500 mV	(depends on detector type)
R_{Det}	= 10^{12} - 10^{16} Ω	(depends on detector photocurrent)
$R_{Feedback}$	= 2.10^{10} Ω	
R_d, R_S	= 100 kΩ	
FETs: g_m	= 10^{-3} A.V^{-1}	
A (OP-27)	= 10^6	
Harness length :	5 m	

The TIA is a feedback amplifier, and operates as a voltage-to-current converter by forcing the detector current to flow through the feedback resistor. It has two main advantages. First, the detector bias is constant regardless of the detector impedance. Therefore, it is independent of the photocurrent, which can change by orders of magnitude depending on the source and observing mode. Secondly, the speed of response is determined not by the large $R_{Det}C_{Det}$ time constant of the detector and its capacitance, but by the much smaller R_FC_F of the feedback resistor and its self capacitance. This allows operation at modulation frequencies of 100 Hz or more. If R_F is much less than R_{Det}, then the output noise is dominated by the Johnson noise of R_F (assuming the FET noise is smaller). Under these conditions, since the signal is proportional to R_F, the output S/N is proportional to $(R_F)^{1/2}$.

The disadvantage of the TIA is that the overall sensitivity is determined by R_F, and not by the detector. R_F cannot be increased arbitrarily because this would eventually compromise the speed of response. Another practical problem is the tendency of high-value resistors to exhibit 1/f noise. Values much greater than a few times 10^{10} Ω are not feasible in practice. Since this is much smaller than the highest (i.e., lowest background) LWS detector impedances of more than 10^{15} Ω, it is the noise of R_F that limits the sensitivity.

Low background tests on LWS prototype detectors resulted in measured NEP values of about 3.10^{-17} W.Hz$^{-1/2}$ in TIA mode. This is considerably inferior to the true sensitivity of the detectors.

Space-borne infrared detectors are sensitive to ionising radiation - mainly gamma rays from Bremsstrahlung emitted when trapped protons and electrons in the earth's radiation belts interact with the spacecraft, and cosmic rays. Ionising events cause spikes in the detector output. With a TIA readout, the spikes decay with a time constant equal to $R_F C_F$. These spikes can be removed by on-board de-glitching hardware, as was implemented on IRAS (Emming et al., 1983; Long and Langford, 1983), or by software if the sampling rate is made high enough. For IRAS, each spike event resulted in an effective interruption of the data lasting about 10 ms. With a hit-rate of 10 per second, this constituted only a 10% inefficiency.

4. The Integrating Amplifier (IA)

A more suitable form of readout for very low background applications is the Integrating Amplifier (IA), which is equivalent to a TIA with an infinite value of R_F. A dual JFET integrating amplifier was developed by Infrared Laboratories (Tucson, Arizona), in the late 1980s, and is now available commercially as a space-qualified component. The device is described by Low (1984) and Low and Alwardi (1986). In the IA, the detector photocurrent charges up a capacitance at the amplifier input. The IR Labs JF4 integrating amplifier uses Silicon JFETs, mounted on a thermally isolated substrate, contained inside a standard TO5 can, which can be mounted at helium temperature.

The JF4 circuit diagram is shown in Figure 5. The FETs are heated to the optimum temperature of about 60 K by passing the appropriate current through the 6 kΩ heater resistor. The total power dissipation of the JF4 device is about 100 μW. The dissipation in the detector itself is negligible (less than 1 pW). The output impedance of the JF4 is about 100 kΩ. The detector current is integrated at the approximately 7.5 pF capacitance (C_I) at the input of FET 1, connected as a source follower with a gain k, of about 0.9. The resulting voltage ramp is measured non-destructively, at the output, and is given by:

$$dV/dt = (k / C_I)\, I_{Det} \qquad (1)$$

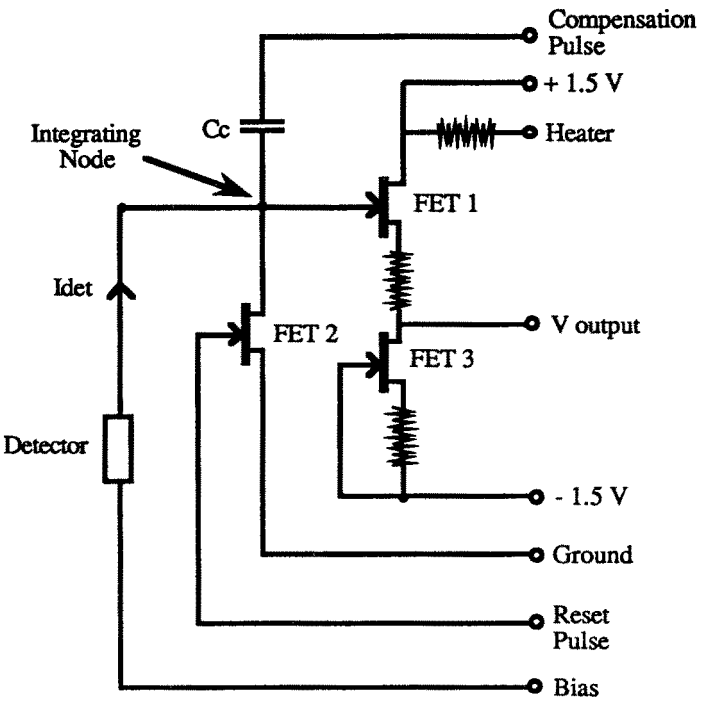

Figure 5

Circuit Diagram of the JF4.

Infrared Laboratories.

After an integration, the accumulated charge must be removed by resetting the input voltage to zero, which involves grounding the integrating node by switching on FET 2. Due to imperfect matching of the FETs, the JF4 has a DC output offset voltage, which varies from one unit to another, in the range ± 10 mV. The reset process itself tends to deposit some charges at the input. This can be neutralised by the simultaneous application of a pulse, of opposite polarity and adjustable amplitude, via the 1-pF "compensation" capacitor, C_C.

During the integration, the input voltage is increasing as the $R_{Det}C_I$ circuit charges up. Therefore the effective bias voltage is changing. Since responsivity is a strong function of bias voltage with these detectors, the integration time must not be too long to avoid non-linearity. In operation, the maximum allowed change in voltage during an integration is kept less than a few % of the detector bias voltage, and a second-order curve is fitted to the ramp to recover the true signal if there is mild non-linearity.

The noise of an integrating amplifier is usually expressed in terms of the "read noise" (e.g., Low and Alwardi, 1986). This is the rms uncertainty in the measured charge at the input due to the noise of the FET. For a wide range of integration times (100 ms to many seconds), the read noise of the JF4 is almost independent of integration time, with a value of typically 15 electrons. It can therefore measure any charge presented at its input with this uncertainty. When used with a photoconductive detector, the measured charge is the detector current integrated over the interval since the previous reset. The LWS detectors have dark currents of typically several hundred electrons/second. The JF4 read noise is such that the statistical fluctuation in the accumulated charge from this dark current will exceed it if the integration time is longer than about a second. Detector noise limited operations is thus feasible with realistic integration times. LWS performance tests have shown that NEPs of about 10^{-18} W.Hz$^{-1/2}$ can be achieved (Griffin et al., 1990, Church et al., 1992). This is more than an order of magnitude better than the sensitivities achieved in TIA mode.

The detector current may be recovered from the IA signal by measuring the voltage change over the known integration time. The JF4 has the advantage that its output can be monitored non-destructively during the integration. It can therefore be sampled regularly, and a straight line fitted to the output voltage ramp. This allows for easier detection of glitches or any other non-linearities in the signal. Ionising events in the detector result in the instantaneous deposition of packets of charge (typically several thousand electrons) at the input, resulting in "jumps" in the output voltage. Since it is not possible to remove the charge without resetting, the data cannot be de-glitched using hardware. Therefore, it is necessary to identify and eliminate the glitches by software.

Clearly, the large increase in sensitivity constitutes a compelling case for the IA, rather than the TIA in very low background applications. However, it would not have been possible to make use of this potential improvement with the orbit originally intended for ISO. This was to be a 12-hours elliptical orbit (1000 - 39400 km) with an Ariane-2 rocket. The ionising hit rate on the 1-mm^3 detectors in this orbit would be 10 per second. IRAS-type TIA amplifiers and de-glitching circuits could easily cope with such a spike rate, with a minimal loss of sensitivity and observing efficiency. With an IA readout, however, the reset interval would need to be severely curtailed, to avoid non-linear effects and allow reliable slope-fitting. This would result in much reduced sensitivity at very low signal levels, as the integration time must be on the order of one second or more to allow the shot noise of the integrated detector current to exceed the amplifier noise. In addition, ionising radiation is known to produce memory effects and excess noise in the detectors (Blum et al., 1990, Price et al., 1992), which could cancel the increase in sensitivity gained by using the IA.

Studies of the four ISO instruments suggested that substantial improvements in performance could be made by flying the satellite in a higher orbit. It was therefore decided to launch ISO into a 24-hour elliptical orbit (1000 - 70000 km) with an Ariane-4 rocket. This reduces the ionising hit rate on the LWS detectors to about 0.1 hits per second for most of the orbit (Metcalfe and Kessler, 199*). Thus, it allows the increase in sensitivity offered by the IA to be realised. When operating at very low source flux levels, the optimum time interval for the LWS detectors is typically four seconds (Church et al., 1992).

5. The LWS Detector Signal Chain

Figure 6 shows the overall configuration of the analogue electronics associated with one detector. The settings of the reset, bias, compensation, illuminators, heaters and thermistors circuits, and also of the detector signal chain and the power supplies, are controlled by the on-board software implemented in the DPU (Digital Processing Unit). The corresponding command electronics and the signal chain are located in the APU.

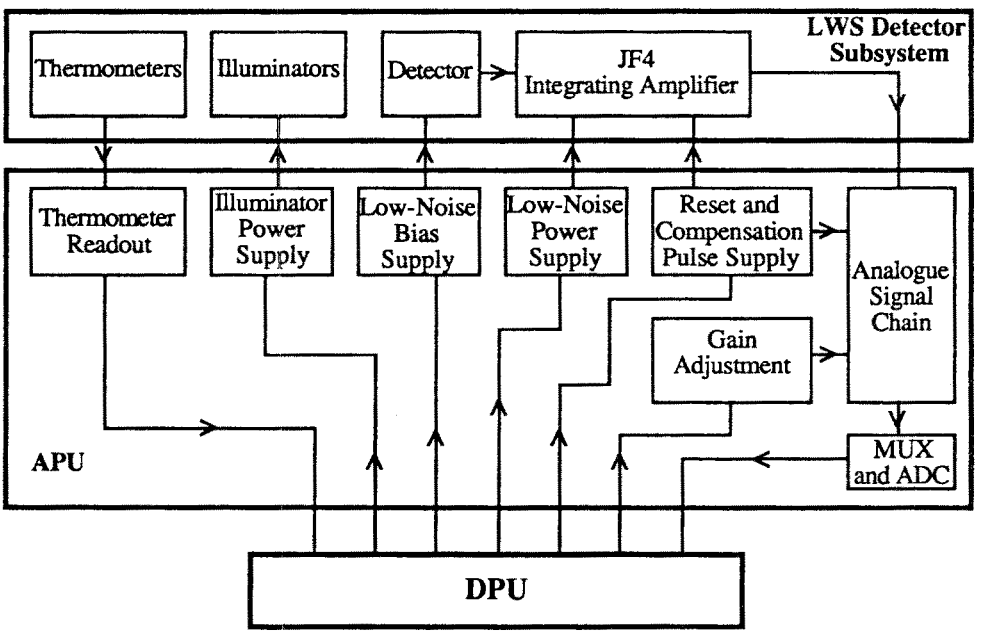

Figure 6

Overall Electronic of the IA Circuit.

The complete detector signal chain is shown in Figure 7, which illustrates the essential functions for one detector. The detector signals are amplified and filtered before being multiplexed with the other detector channels, and sampled by a 12-bit ADC.

In the LWS, each detector output is sampled at 132 Hz. This is the highest frequency that can be used, determined by the available telemetry rate, and is much higher than is necessary to recover the quiescent signal levels, but allows glitches or any other non-linearities in the output voltage ramp to be more easily recognised. The LWS data processing software allows slope computations to be made on de-glitched ramps, so that loss of integration time due to glitches is minimised. There is no further signal processing on-board: all detector samples are transmitted to the ground-station.

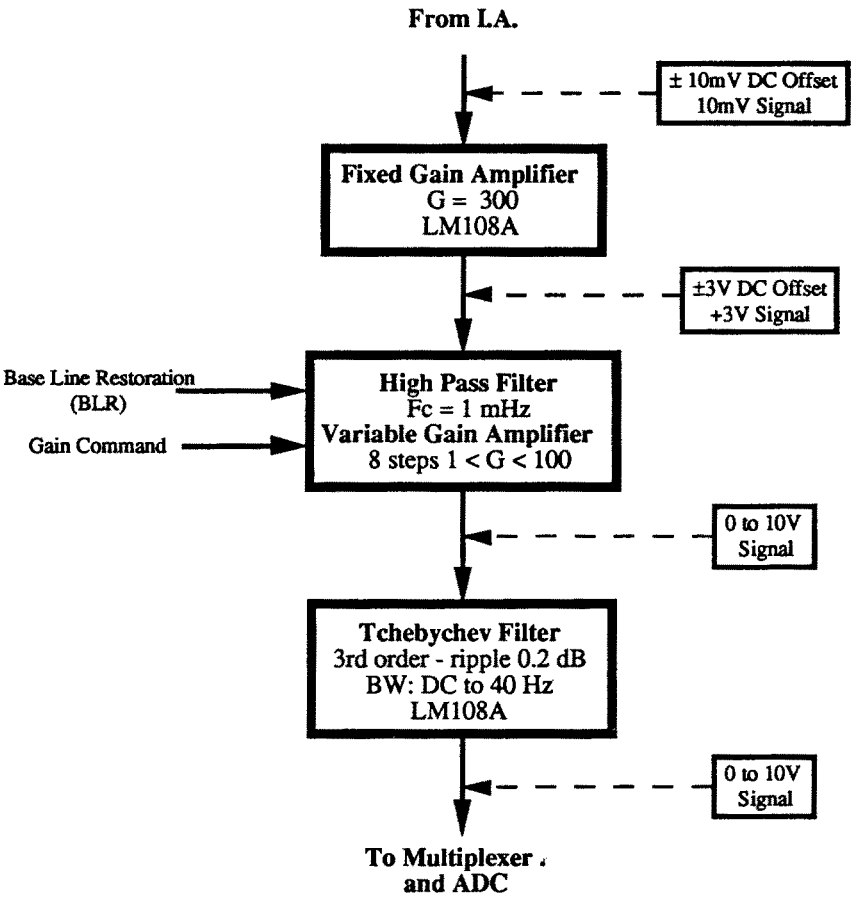

Figure 7

Analogue Electronic Chain associated with each LWS Detector.

Integrating Amplifier Concept.

5.1. DETECTOR AND IA

Each detector bias voltage can be commanded from the ground to any of eight values. There is a stringent noise and stability specification for the bias voltage supply lines (and also for the power supply lines to the JF4 amplifiers) to ensure that the overall noise is dominated by the detector and/or the JF4 itself. Two of the eight selectable bias voltages are bias boost levels, used to cure the detectors after a heavy exposure to ionising radiation. Such a scheme was used successfully on IRAS (Petroff et al., 1979, and Varnell, 1982), and has been shown to work satisfactorily for the LWS detectors (Price et al., 1992). The signal at the output of the JF4 is a voltage ramp with $\Delta V < 10$ mV, superimposed on a fixed DC offset in the range $\pm$ 10 mV. The amplitude of the compensation pulse can be adjusted to make the input voltage equal to 0 V (i.e., output voltage equal to the known DC offset) after the reset pulse. The exact amplitude of the compensation pulse depends on a number of factors: the individual JF4 pair and its exact operating point, the of-stray capacitances in the vicinity of the integrating node, the impedance of the warm-cold interconnection harness, etc...

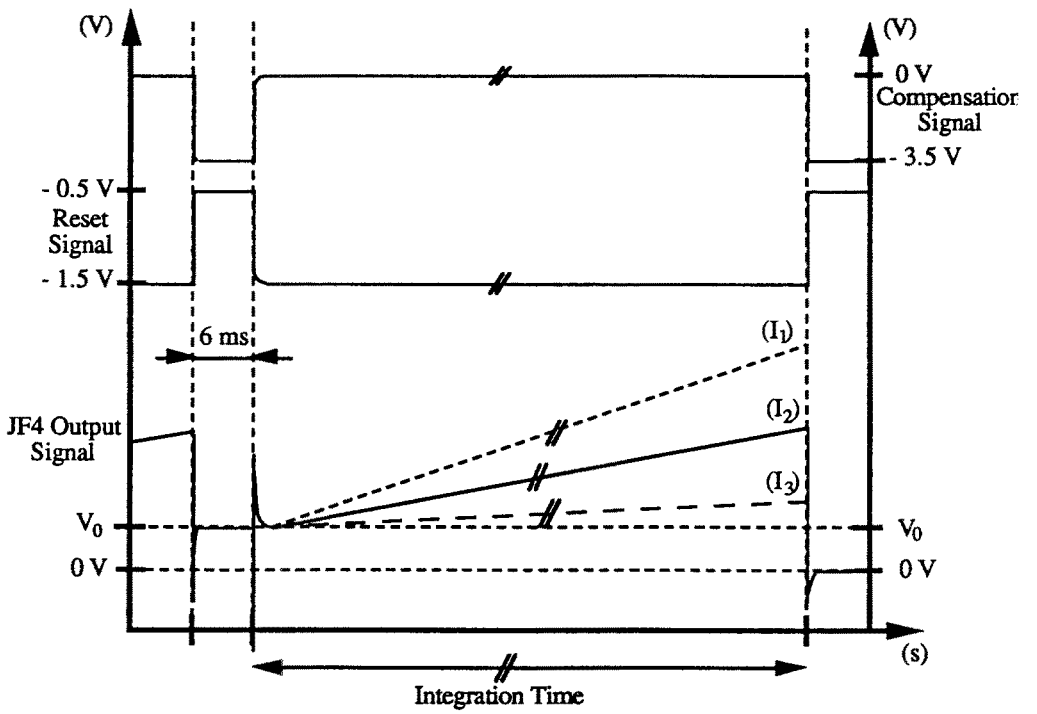

Figure 8

Timing Diagram of the Reset and Compensation Pulses and the JF4 Output.

The required value is generally stable once it has been set; however, to take into account the possibility that it might change in flight due to ageing of components or changes in the harness impedance due to thermal effects, the compensation pulse amplitude is individually adjustable (by ground command) to any of 256 values in the range -2.5 to -4.5 V, for each IA. The reset and compensation pulses are applied simultaneously and both trailing edges have a RC time constant of 170 ± 20 μs. Figure 8 is a theoretical timing diagram of the reset and compensation pulses and the JF4 output signal. The JF4 output offset V_0 is typically a few mV. Three different detector current levels are illustrated, where $I_1 > I_2 > I_3$.

The ± 1.5 V IA power lines for the IA, the bias and compensation lines are all derived from highly filtered, low-noise supplies. This ensures that their voltage noise makes an insignificant contribution to noise at the IA output.

5.2. FIXED - GAIN AMPLIFIER

This is DC-coupled, and has a nominal gain of 300. The output signal is thus a ramp with $\Delta V < 3$ V, superimposed on a fixed offset in the range ± 3 V. This differential amplifier is based on two LM-108 AH chips (see Section 6), with RC filters on both inputs.

5.3. HIGH - PASS FILTER

Although DC-coupling of the entire chain would ideally be preferred, it proved necessary to introduce a high-pass filter to remove the IA output offset. The offset is about a few volts at the fixed-gain amplifier output, and must be removed at this stage if further gain is to be applied, otherwise the following amplifier will saturate. Since this offset can vary from one unit to another, and may be subject to drifts due to IA temperature changes or ageing effects, it would need to be removed by subtraction of a commandable offset. Thus, it requires a separate DAC for each of the ten channels. This option was considered, but proved too expensive in terms of power, mass and volume inside the APU. To achieve AC-coupling, a simple high-pass RC filter with a time constant of 200 seconds is used, giving a cut-on frequency of 0.8 mHz. With this low cut-on frequency, there is negligible distortion of the IA output signal, even for integration times of 10 seconds (distortion around 1.5 %).

Due to the extremely long discharge time of the capacitor, the high-pass filter must be reset simultaneously with the IA at the beginning of each integration, to prevent eventual saturation of the variable-gain amplifier.

This is done using a HI-300 electronic switch, which connects the filter capacitor directly to ground. This command is represented on Figure 7 by the signal BLR (Base Line Restoration).

5.4. VARIABLE - GAIN AMPLIFIER

The output from the high-pass filter is fed to a variable-gain amplifier, based on an OPA-111 operational amplifier (see paragraph 6). Eight gains between 1 and 100, varying on a logarithmic scale, are commandable from the ground. The maximum total gain is thus 30,000. With a 12-bit ADC operating over a 20 V voltage range, at maximum gain one bit corresponds to 8 electrons at the IA input. This level is less than the IA read noise.

5.5. LOW - PASS FILTER

The purpose of the low-pass filter is to prevent noise at frequencies higher than the Nyquist frequency being aliased into the signal band. It also reduces the susceptibility of the full amplification chain to high-frequency interference. The filter is a three-pole Tchebychev design, implemented using a single LM-108 op-amp (see section 6), with a cut-off at 40 Hz. This figure is based on a compromise between maximum rejection of out-of-band noise and minimum settling time of the system after the reset pulse is applied. The output of the low-pass filter is subject to ringing after reset, so that the output takes some time to stabilise. The effect could be calibrated out with a knowledge of the response of the system and the input transient produced by the reset pulse. However, this is made difficult by the fact that the reset transient is found to depend to some extent on the detector impedance (and hence on the signal itself). The standard operating mode will involve a delay of 100 ms before meaningful data samples are taken. With a 40 Hz cut-off, the settling time is about 100 ms. Only a small overhead in observing time will result from this delay: 100 ms is comparable to the settling time of the LWS grating (about 75 ms), and much shorter than the typical LWS integration time (0.5 to 10 seconds). Since the detector data are sampled at 100 Hz and transmitted to the ground, further signal filtering can be carried out digitally if required.

5.6. GENERAL CONSIDERATIONS

A typical scanning operational sequence using only the grating starts with the settings of the different parameters of the grating and of the detector subsystem (bias and compensation levels, operational temperature of the detector block). The grating is then set to the starting position of the scan and the reset and compensation signals are applied to the ten detectors.

The integrations can then be performed, as many as needed, until the next scan step. They are always followed by the application of a reset-compensation signal. They result in voltage ramps that are amplified, filtered and digitised before being sent to ground via the telemetry.

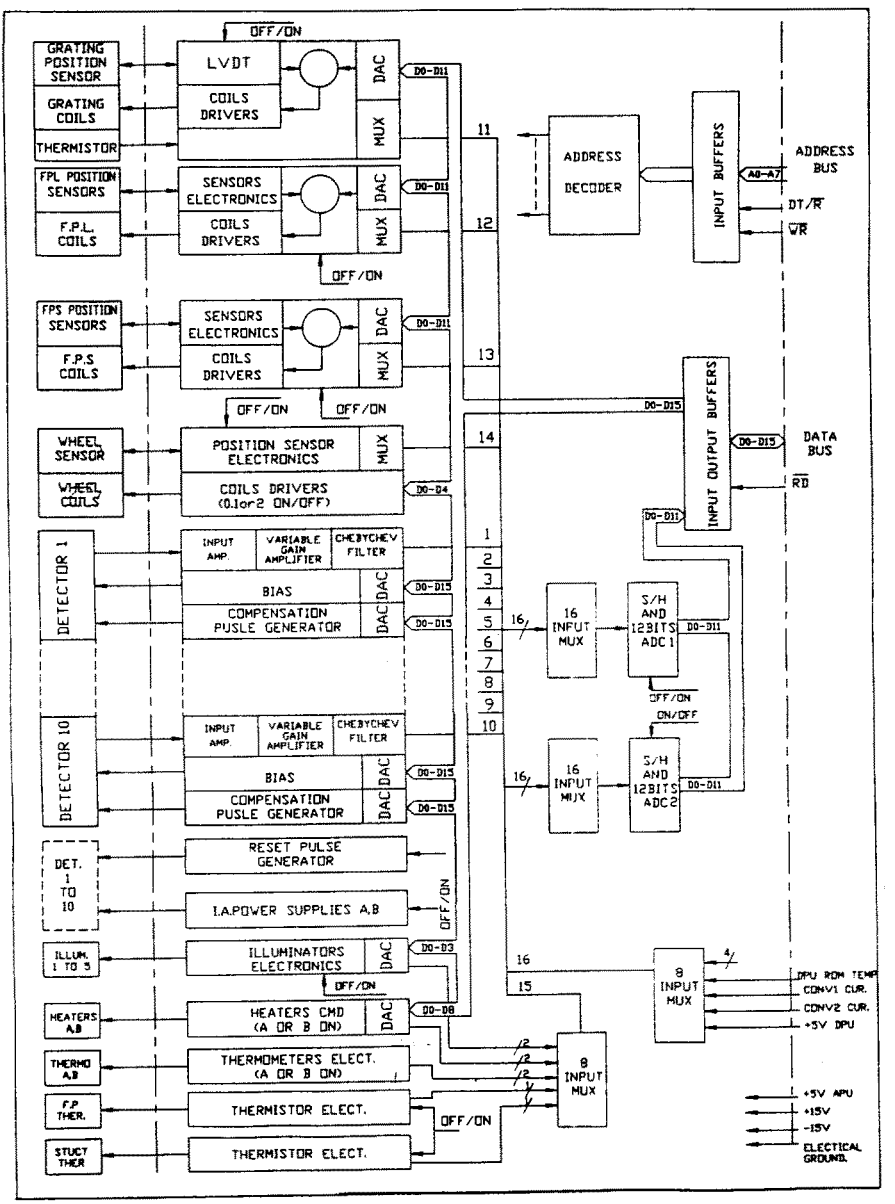

Figure 9

Block diagram of the APU.

Due to the high sensitivity level expected for the LWS detectors, special care has been provided during the overall design of the whole electronics to minimise the susceptibility of the signal chain to electromagnetic interference. For example, a single analogue ground point is implemented in the APU, requiring the electrical isolation of the whole detector block from the sidewall of the instrument. Figure 9 presents an overall block diagram of the APU (Analogue Processing Unit) developed at CESR, in which the detector subsystem electronics can be easily identified.

6. Tests Results

Studies were performed at CESR to find the most suitable operational amplifiers (in terms of noise and power dissipation) to be used at the different stages of the detector amplification chain.

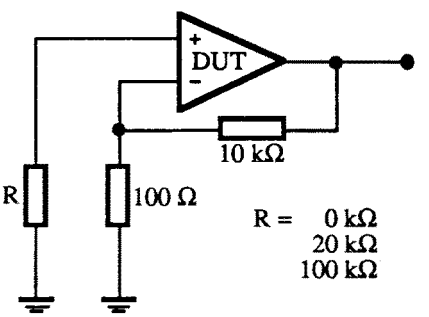

Figure 10

Operational Amplifiers Noise Measurement Test Configurations.

Three different configurations, based on the circuit shown in Figure 10, were tested. The only difference between them is the impedance seen at the input by the amplifier (0 kΩ, 20 kΩ, and 100 kΩ). For these tests a gain of 100 was used, and measurements were carried out on three different types of amplifier (OP-27, LM-108 and OPA-111).

The test results are given in Table 1 (input impedance equal to 0 kΩ) and Table 2 (input impedance equal to 20 kΩ or 100 kΩ). The output noise spectral density was measured at frequencies between 0.1 and 100 Hz. The last line shows the maximum acceptable values specified to ensure that the fixed gain amplifier noise would not degrade the overall performance.

In Table 2, results are given for different impedances, at different temperatures. The values quoted for 60 K are calculated from the measured values of noise (100 kΩ at 300 K) quadratically reduced using the expression $(4kR(300-60))^{-1/2}$.

Table 1

Operational Amplifiers Noise Test Results - Input impedance = 0 Ω.

Noise Densities in $nV.Hz^{-1/2}$.

	0.1 Hz	0.5 Hz	1 Hz	10 Hz	100 Hz
OP - 27	25	17	16	6	4
LM - 108	150	60	50	25	18
OPA - 111	250	80	60	25	11
Project Specifications	< 200	< 100	< 75	< 40	< 25

Table 2

Operational Amplifiers Noise Test Results - Other Configurations.

Noise Densities in $nV.Hz^{-1/2}$.

		0.1 Hz	0.5 Hz	1 Hz	10 Hz	100 Hz
OP - 27	R=100 kΩ T=300 K	3430	1120	930	180	75
	R=100 kΩ T= 60 K	3430	1120	929	176	65
	R= 20 kΩ T=300 K	860	305	208	56	30
LM - 108	R=100 kΩ T=300 K	173	94	75	44	44
	R=100kΩ T= 60 K	169	86	65	25	25
	R= 20 kΩ T=300 K	110	66	55	29	24
OPA - 111	R=100 kΩ T=300 K	286	105	78	43	43
	R=100 kΩ T= 60 K	284	98	69	23	23
	R= 20 kΩ T=300 K	260	88	66	29	22
Project Specifications		< 200	< 100	< 75	< 40	< 25

Considering the 100 kΩ output impedance of the IA, and the roughly 50 Hz frequency range, these results suggest that the LM-108A is the best choice for the fixed-gain amplifier and the Tchebychev filter. It has the further advantages of being qualified for space applications, and has a very low power dissipation. It is worth noting that, for small input impedances, the OP-27 has the lowest noise. Other measurements we have made, not reported here, show that for high values of source impedance (1 MΩ or more), the OPA-111 is best. It was therefore chosen for the variable-gain amplifier.

Tests were also performed at CESR on a complete electronic breadboard, fully representative of the APU detector signal processing chain. For those noise measurements, the JF4 component was simulated by its output impedance, i.e. a 100 kΩ grounded resistor. All this chain was placed in a Faraday cage. The results, taken at the end of the chain, were read on a HP-3562A spectrum analyzer, placed outside the cage. Measurements were performed at 300 K.

Results are summarised in Table 3, which also gives the figures for a 100 kΩ impedance placed at 60 K (calculated from the 300 K results, as for Table 2). A quick comparison with the project specifications shows that the noise of this electronics chain is within the specifications, except for the highest frequencies where the levels are a bit higher.

Table 3

Noise Test Results performed on the overall detector electronics breadboard.

Noise Densities in $nV.Hz^{-1/2}$.

Frequency (Hz)	T=300 K	T=60 K	Project Specifications
0.1	200	193	< 200
0.5	100	93	< 100
1	73	63	< 75
10	55	40	< 40
100	50	35	< 25

To illustrate the output of the analogue chain, Figure 11 shows a typical signal output for a series of integration ramps, recorded using the LWS Flight Model. The output has been scaled to represent the IA output voltage. The detector current is about 30,000 electrons per second.

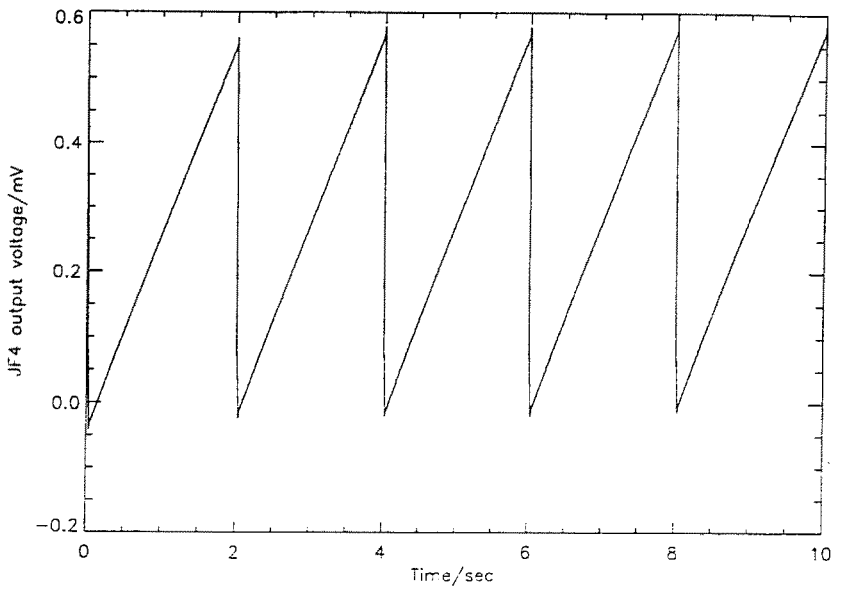

Figure 11

Typical Integration Ramp.

Conclusions

We have outlined the two main signal-readout methods used with infrared photodetectors. We have also shown how, for low-background space applications, the use of an Integrating Amplifier type readout allows higher sensitivity to be achieved than using the more traditional TIA circuit. The Integrating Amplifier configuration was therefore adopted for the ISO-LWS detectors, and a signal processing chain which allows for detector noise limited operation was designed and implemented. It is likely that this form of readout will become the standard in future satellite missions with cooled telescopes. To gain the advantage in sensitivity offered by the IA, it is necessary to operate in an orbital environment in which the ionising radiation background is as low as possible (high apogee orbit). To our knowledge, it will be the first time that such IAs will be used with Ge:Ga photoconductors in a space experiment.

Acknowledgements

We should like to thank for their contribution to this work the members of the LWS Consortium lead by Prof. P.E. Clegg, P.I. of the LWS experiment. This development project has required a close collaboration between CESR and QMW laboratories. In particular, we should like to thank at CESR the technical team lead by F. Cotin, with J. Landé and M. Ehano and the scientific team, E. Caux and G. Serra, and at QMW, P. Ade, A.G. Murray, M.C. Price, F.D. Robinson and D. Vickers.

Finally, thanks also to Centre National d'Etudes Spatiales (CNES) and the U.K. Science and Engineering Research Council (SERC) for their financial support.

References

* Blum J., Hajduk Ch., Lemke D., Salama A., Wolf J., 1990, " High-energy radiation effects on the ISOPHOT far-infrared detectors ", Infrared Physics, 30, 93.

* Church S.E., Griffin M.J., Ade P.A.R., Price M.C., Emery R.J. and Swinyard B.M., 1992, " Performance testing of doped-germanium photoconductors for the ISO Long Wavelength Spectrometer ", Proceedings of the ESTEC Symposium on Photon Detectors for Space Instrumentation, ESA SP-356, ESTEC, Nov. 10-12 1992 (in press).

* Eggel H. et al., 1990, " The Scientific Instruments for ISO - Technical Highlights ", ESA Bulletin No. 61.

* Emery R.J. et al., 1987, " The ISO Long Wavelength Spectrometer ", PROC. SPIE, 589, 194.

* Emery R.J., Church S.E., King K.J. and Swinyard B.M., 1993, " Testing the Long Wavelength Spectrometer for ISO ", presented at the SPIE Aerospace Science and Sensing Conference, Orlando, Florida, 14-16 April 1993.

* Emming J.G., Arentz R.F., Downey C.H., Long E.C., Smeins L.G., 1983, " Pulse circumvention circuit for the infrared astronomical satellite telescope ", Instrumentation in Astronomy V, Vol.445, pp.254-262, Proceedings of the 5th Meeting, London.

* Griffin M.J.G., Ade P.A.R., Church S.E., Murray A.G., Overhamm M., Faymonville R., Su Ying W., 1990, " Performance Tests on Ge:Ga and Ge:Be Detectors for the ISO Long Wavelength Spectrometer ", Proceedings of the 29th Liège Colloquium " From Ground-Based to Space-Borne Submillimetre Astronomy ", D Reidel.

* Langford D.L., Simmonds J.J., Ozawa T., Long E.C., Paris R., 1983, " Infrared and visible detector electronics for the Infrared Astronomical Satellite (IRAS) ", Instrumentation in Astronomy.V, Vol.445, pp.244-253, Proceedings of the 5th Meeting, London.

* Long E.C. and Langford D.L., 1983, " Test Results and in-orbit operation of the Infrared Astronomical Satellite Circumvention circuit ", Instrumentation in Astronomy V, Vol.445, pp.264-271, Proceedings of the 5th Meeting, London.

* Low F.J., 1981, " Application of JFets to low background focal planes in space " SPIE Vol. 280 Infrared Astronomy-Scientific/Military Thrusts and Instrumentation.

* Low F.J., 1984, " Integrating amplifiers using cooled JFETs ", Applied Optics, Vol. 23, No. 9, pp.1308-1309.

* Low F.J. and Alwardi M., 1986, " Progress in the development of Integrating JFET amplifiers ", Proceedings of the Second Infrared Technology Workshop, NASA - TM 88213.

* Luinge W. et al., 1980, " Evaluation of Si:As photoconductive detectors for infrared astronomy ", Infrared Physics, 20, 39.

* Metcalfe L. and Kessler M.F., 1992, " Scientific capabilities of the ISO payload ", ESA Document, ID: ISO-SSD-8805, ESA ESTEC Astrophysics Division.

* Petroff M.D., Pickel J.C. and Curry M.P., " Low-level radiation effects in extrinsic infrared detectors ", 1979, IEEE Transactions on Nuclear Science, NS-26 n° 6, 4840.

* Price M.C., Griffin M.J., Church S.E., Murray A.G. and Ade P.A.R.,1992, " Ionising radiatio-induced effects in doped germanium photoconductors ", Proceedings of the ESTEC Symposium on Photon Detectors for Space Application, ESTEC, Nov. 10-12 1992 (in press).

* Varnell L., " Radiation effects in IRAS extrinsic infrared detectors ", 1982, IEEE Transactions on Nuclear Science, NS-29 n° 6, 1551.

* Young E.T., Rieke G.H., Gautier T.N., Hoffmann W.F., Low F.J., Poteet W., Fazio G.G., Koch D., Traub W.A., Urban E.W., Katz L., 1981, " Test results of Spacelab 2 infrared telescope focal plane ", SPIE Vol. 280 Infrared Astronomy-Scientific/Military Thrusts and Instrumentation.

* Young E.T., 1983, " Photoconductive Detectors for Space I.R. Astronomy " Adv. Space Res. Vol.2, No .4, pp.59-68.